High Power Factor with Compositional and Temperature Stability in $(Ca_xSr_{1-x})Si_2$ Thin Films near Room Temperature

Kodai Aoyama[1], Takao Shimizu[1,2], Takayoshi Katase[3], Yoshisato Kimura[1], and Hiroshi Funakubo[1]*

[1]School of Materials and Chemical Technology, Institute of Science Tokyo, 4259 Nagatsuta, Midori-ku, Yokohama 226-8501, Japan

[2]Research Center for Functional Materials, National Institute for Materials Science, Tsukuba 305-0044, Japan

[3]MDX Research Center for Element Strategy, Institute of Integrated Research, Institute of Science Tokyo, 4259 Nagatsuta, Midori-ku, Yokohama 226-8501, Japan

ABSTRACT

The effects of Ca content (x) on the crystalline phases and thermoelectric properties of the $(Ca_xSr_{1-x})Si_2$ films were investigated. The solubility limit of the cubic phase was found to be narrow, with $x = 0.08$, compared to that of arc-melted samples. For $x \geq 0.17$, a mixed phase was observed, which included a layered structure not previously reported in the arc-melted samples. In both the single cubic-phase region and the mixed-phase regions, the electrical resistivity and Seebeck coefficient varied systematically with x at 323 K. Consequently, a high power factor of approximately 1000 $\mu Wm^{-1}K^2$ was achieved over a wide composition range (x = 0.03 to 0.17) at 323 K. The wide compositional tolerance for a high power factor is advantageous for practical fabrication and offers robustness against compositional fluctuations. In addition, the power factor remained above 850 $\mu Wm^{-1}K^{-2}$ within the temperature range of 223 K to 373 K for x = 0.04 to 0.13. These results highlight that $(Ca_xSr_{1-x})Si_2$ films with a predominantly cubic phase are promising candidates for thermoelectric applications near room temperature due to their high power factor across a broad range of compositions and temperatures. Furthermore, the highest power factor of 2000 $\mu Wm^{-1}K^{-2}$ was achieved at 210 K for the film with x = 0.04, which consisted solely of the cubic phase. The value exceeds that of previously reported $SrSi_2$ films prepared using the same sputtering method.

KEYWORDS Thermoelectrics, Electronic property, Crystal structure, Silicide, Sputtering.

Introduction

With the proliferation of Internet of Things (IoT) devices, edge computing is expected to experience significant growth in the near future[1]. There are two main power supply methods for such devices: power outlets and batteries. When using power outlets, device placement is limited by outlet locations, and power is often supplied more than actual requirements. Conversely, battery-powered devices contribute to increased battery disposal, raising environmental concerns. To deploy IoT devices in an eco-friendly manner, alternative power supply methods such as energy-harvesting should be considered. Thermoelectric systems represent one promising solution to these power supply challenges[2]. They offer advantages such as compact design, high conversion efficiency for small-scale heat sources, solid-state operation, and extended operational lifetimes with minimal maintenance requirements[3]. It is also expected to be used as a Peltier device for cooling. Cooling devices are more promising applications in the case of TE thin films. The low efficiency of these thermoelectric devices restricts their practical application, particularly for operations near room temperature[4]. Furthermore, materials with good thermoelectric properties often contain rare and toxic elements. For example, the Bi-Te-Se system is one of the most widely investigated thermoelectric materials for use near room temperature[5]. Therefore, it is necessary to develop alternative materials that exhibit good thermoelectric performance near room temperature while comprising nontoxic and widely available elements. The efficiency of thermoelectric materials is directly related to the dimensionless figure of merit (ZT), defined as $ZT = S^2\rho^{-1}\kappa^{-1}T = S^2\sigma\,\kappa^{-1}T$, where S, ρ, σ, κ, and T are the Seebeck coefficient, the electrical resistivity, the electrical conductivity, the thermal conductivity, and the absolute temperature, respectively[4]. The electrical property term ($S^2\rho^{-1}$) in ZT, is known as the power factor, is critical for achieving high thermoelectric performance. It is

worth noting that thermal conductivity has been reported to decrease when nanostructures are introduced[3,6–10]. This suggests that once a material with a high power factor is discovered, its overall *ZT* can be further improved through microstructural engineering aimed at reducing thermal conductivity.

Considering both thermoelectric performance and environmental impact, silicide-based compounds have emerged as promising candidates for thermoelectric applications[11]. These compounds offer advantages such as low environmental impact, abundant constituent elements in the Earth's crust, and excellent compatibility with Si-based fabrication processes. This compatibility is especially beneficial given the increasing heat generation in computing systems driven by rising energy consumption[12,13].

Among silicides, $SrSi_2$ with a cubic structure, (space group $P4_332$, hereafter described as the cubic phase) has shown particular promise as a thermoelectric material. It has been reported to exhibit a high power factor near room temperature, alongside eco-friendly characteristics[6,14–18]. Another form of $SrSi_2$ is a metastable layered structure (space group $P\text{-}3m1$, hereafter described as the layer phase), which exhibits lower electrical resistivity and higher carrier density than the cubic phase at temperatures below room temperature[19–21]. In our study of the layer phase of $Ca_xSr_{1-x}Si_2$, regardless of composition, the layer phase exhibited metallic behavior with low ~~and~~ electrical resistivity that increased with increasing temperature.[23] Our previous work demonstrated that thermoelectric properties can be improved by combining the layered and cubic phases[22]. The optimal power factor was observed when the electrical resistivity and Seebeck coefficient were lower than those of $SrSi_2$ alone. The mixed-phase film was achieved by precise control of the deposition temperature, as the phase composition of the film is highly sensitive to deposition conditions[22]. The band structure of $Ca_xSr_{1-x}Si_2$ was investigated, and it was suggested

that as Ca was solid-solvated, the intersection between the minimum of the conduction bands and the maximum of the valence bands along the Γ−*X* direction, and the density of states near the Fermi level increased.[36] An increase in the density of states near the Fermi level may lower the electrical resistivity and Seebeck coefficient compared to $SrSi_2$. Therefore, $Ca_xSr_{1-x}Si_2$ has optimal lower electrical resistivity and Seebeck coefficient than $SrSi_2$ and may have improved power factor. Furthermore, we have confirmed that the layer phase becomes the main phase when the Ca content is high in $(Ca_xSr_{1-x})Si_2$ thin films.[23] This suggests that an optimal two-phase coexistence film with high thermoelectric properties can be realized by controlling both the deposition temperature and the *x* value in $(Ca_xSr_{1-x})Si_2$. Additionally, Ca-substituted $(Ca_xSr_{1-x})Si_2$ has been reported to exhibit improved thermoelectric properties. Specifically, power factor enhancement has been observed upon substituting Sr with Ca.[24] However, systematic research on $(Ca_xSr_{1-x})Si_2$ over a wide range of *x* values remains limited.

In this study, we investigate the effect of the Ca content (*x*) on the constituent phase and electrical properties of $(Ca_xSr_{1-x})Si_2$ thin films deposited on (001) Al_2O_3 substrates using the RF magnetron sputtering method. As a result, the films with thermoelectric power factors exceeding 1000 $\mu Wm^{-1}K^{-2}$ at 373 K were obtained over a wide composition range (x = 0.03-0.17), encompassing both the single cubic-phase region and the mixed phase region comprising cubic and layered structures. These power factors surpass those reported for the Bi-Te-Se system, including $Bi_{0.99-x}Sn_xTe_{0.4}Se_{0.6}$, and $Bi_{0.99}Te_{1-x}Se_x$[5].

Furthermore, the highest power factor of 2000 $\mu Wm^{-1}K^{-2}$ was achieved at 210 K for the film with x = 0.04, which consisted solely of the cubic phase. The value exceeds that of previously reported $SrSi_2$ films prepared using the same sputtering method[22,23,25,26]. Moreover, the power factor for x = 0.04 to 0.13 remained above 850 $\mu Wm^{-1}K^{-2}$ across a wide temperature range from

223 K to 373 K, encompassing near room temperature conditions. These findings indicate that $(Ca_xSr_{1-x})Si_2$ films with a predominantly cubic phase are promising candidates for thermoelectric applications near room temperature, due to their high and stable power factor across both composition and temperature ranges.

Methods

$(Ca_xSr_{1-x})Si_2$ films with thicknesses ranging from 0.75–1.4 μm were prepared on (0001) Al_2O_3 substrates using the RF magnetron co-sputtering method in an Ar atmosphere containing 5% H_2. Arc-melted samples of $SrSi_2$ and $CaSi_2$ were used as co-sputtering targets. The deposition temperature, deposition pressure, and target-substrate distance were set to 973 K, 100 m Torr, and 60 mm, respectively. To control the Ca content (x value), the RF power applied to the $CaSi_2$ target was varied from 0 to 50 W, while the power applied to the $SrSi_2$ target was maintained at 50 W.

The x values of the deposited films were measured using X-ray fluorescence spectrometry (XRF; PANalytical, PW4400). The (Ca+Sr)/Si ratio in all films was approximately 0.5. The constituent phases of the films were characterized using X-ray diffraction (XRD; Bruker AXS, D8 DISCOVER). XRD 2θ-θ scans were conducted by changing the sample inclination angle (ψ), with continuous sample rotation. Integrated 2θ-θ scans were obtained by integrating the diffraction intensities along the ψ direction[27].

The temperature dependence of electrical resistivity was measured using the 4-point method, while the Seebeck coefficient was measured in a helium (He) atmosphere under reduced pressure

over the temperature range of 323 K to 673 K using a ULVAC ZEM-3 system. For measurements below room temperature (10 K to 300 K), resistivity and Hall effect measurements were performed using the Van der Pauw 4-probe method, while the Seebeck coefficient was measured under steady-state conditions in a vacuum (pressure < 1×10^{-5} Pa). The thermoelectromotive force (ΔV) and temperature difference (ΔT) were measured simultaneously by applying a ΔT of up to 2.0 K in the in-plane direction. It must be noted that the discontinuity of the obtained data were observed at 300K. This is considered to be mainly due to the measurement setups for these two temperature regions. The size of the sample for the measurement is different; the low-temperature side measurement used 10 mm × 10 mm, while the high-temperature side used 15 mm × 5 mm. Imperfection in the shape of the measurement samples and inhomogeneity of the film thickness and the film composition affect the discontinuity in the measured data at 300 K. Imperfection of the sample shape may also affect the obtained results. The Seebeck coefficient was then calculated from the slope of the ΔV–ΔT plots[28]. Due to the different sample geometries required for measurements below and above room temperature, two sets of films were deposited simultaneously. The identical x values of these films were confirmed by XRF analysis.

Results and discussion

Ca content dependence of constituent phases in $(Ca_xSr_{1-x})Si_2$ films

Figure 1(a) and (b) shows the integrated XRD 2θ-θ scan results for films with different x values. The XRD patterns for films with $0 \leq x \leq 0.13$ indicate the presence of a single cubic phase, which corresponds to the stable phase in $SrSi_2$[18]. As the x value increases beyond this

range, the layered phase begins to emerge; however, the cubic phase remains dominant in films with $x = 0.17$. At $x = 0.20$, the layer phase becomes the major constituent. Thus, in the composition range $x = 0.17$–0.20, the films consist of mixed phases comprising both cubic and layered structures.

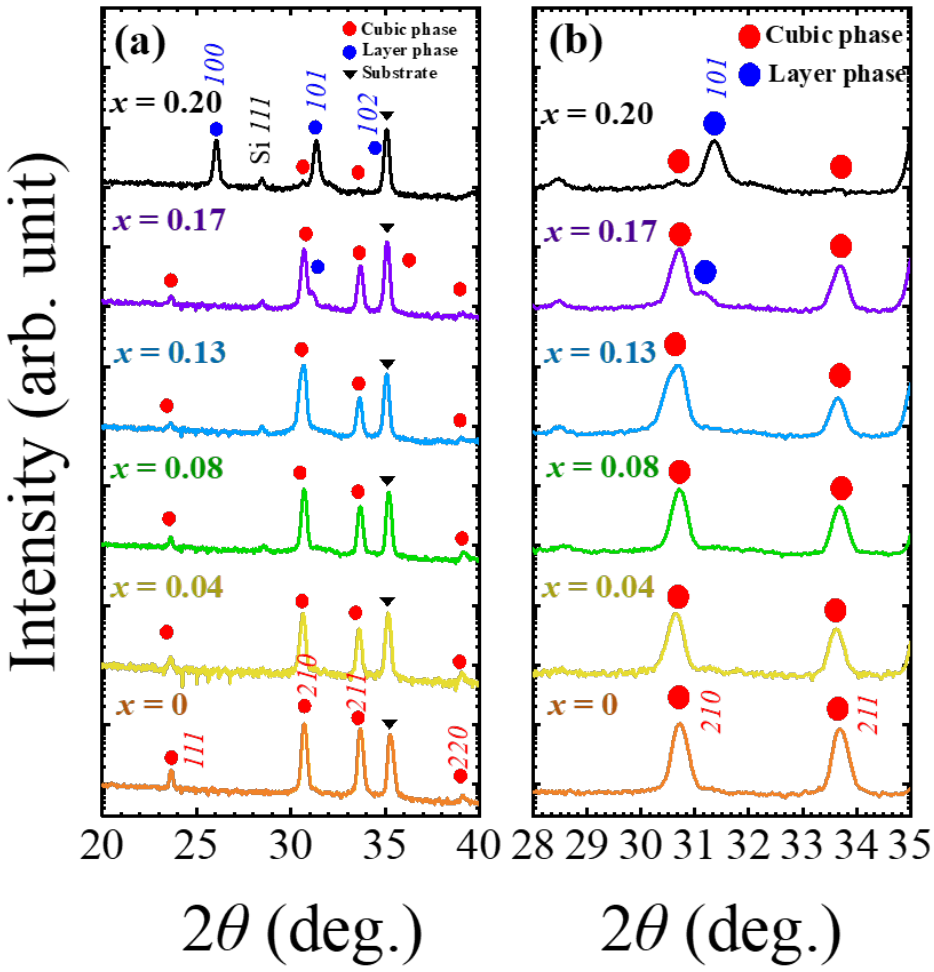

Figure 1. Integrated XRD profiles of (a) $2\theta = 20$-$40°$and (b) $2\theta = 28$-$35°$for $(Ca_xSr_{1-x})Si_2$ films with various x values deposited at 923 K. Inverted triangles show the peaks from the Al_2O_3 substrates.

Figure 2 shows the lattice constants of $(Ca_xSr_{1-x})Si_2$ as a function of x. The lattice constants were calculated by integrating the value of ψ over the range from 0 to 30°. In this range, only the cubic crystal peak (210) exists. In the range from ψ = 30° to 40°, the layer phase peak (101) exists, so it was excluded. For comparison, previously reported data for $(Ca_xSr_{1-x})Si_2$ prepared by annealing arc-melted samples at 1073 K in vacuum-sealed quartz tubes for three days are also plotted (Figure 2)[24]. The lattice constant decreases with increasing x up to x = 0.08, after which it remains nearly constant up to x = 0.17. Since all films were deposited at the same temperature, it is assumed that the effect of the thermal stress is independent of the x value of the films. Nevertheless, the fact that the lattice constant of the cubic phase decreases proportionally with the x value up to x = 0.08 is due to the effect of the substitution of Ca, which has a smaller ion radius, being substituted for Sr sites following the Vegard's law. When x > 0.08, the fact that the lattice constant does not change with x value means that Ca was not substituted for Sr sites. In contrast, earlier reports demonstrated a monotonic decrease in lattice constant up to x = 0.15, as shown in Fig. 2[24]. This difference indicates that the Ca solubility in the present study is lower than that of the arc-melted samples, despite the absence of identifiable XRD peaks corresponding to the layer phase (see Fig. 1). A minor fraction of the layered phase may suppress peak observation in the film with x = 0.13[24]. Furthermore, the volume fractions of the cubic and layered phases might be varied in the films with x = 0.13 and 0.17, as inferred from changes in the XRD patterns shown in Fig. 1. Cubic in a mixed phase is independent of the second layer phase because its lattice constant does not change even when its volume decreases. In this composition region, lattice parameter of cubic phase does not change because the composition of cubic phase keep almost onstant within this region.

According to our previous study for $SrSi_2$ thin films, form a cubic phase and a layer phase (trigonal structures) coexisting between 873 and 973 K[22]. On the other hand, when $CaSi_2$ is deposited under the same conditions, we have confirmed that a rhombohedral structure (layer, but stacking is different) is formed at 973 K and a layer phase (trigonal structures) is formed at 873 K.[23] This observation suggests that the difference in formation free energy between the layer and cubic phase of $SrSi_2$ is smaller in the thin films than in arc-melted samples. In contrast, the difference in formation free energy between cubic and layer phase of $CaSi_2$ is at least larger than that in $SrSi_2$ because the cubic phase cannot be confirmed under the same deposition conditions. In addition, density functional theory (DFT) calculations show that for $SrSi_2$, the cubic phase is slightly more stable than the layer phase, whereas for $CaSi_2$, the layer phase is more stable than the cubic phase.[31] Therefore, it can be assumed that increasing the Ca content per unit cell improves the stability of the layer phase. In thin films, this results in the layered phase becoming more stable than the cubic phase at lower Ca concentrations than in the arc-melted samples, narrowing the solid-solution region in the thin film, as shown in Fig. 2. In other words, the constituent phases of films with compositions above $x = 0.08$ would separate into a cubic phase with $x = 0.08$ and a layered phase with $x \sim 0.20$. As shown in Fig.2, the lattice constant of the $(Ca_xSr_{1-x})Si_2$ thin film is smaller than the value reported for arc-melted samples[24]. Since the linear thermal expansion coefficient of (001) Al_2O_3 is smaller than that of $SrSi_2$, an in-plane tensile strain is imposed on the film during the cooling process, causing the lattice constant of the film to expand in-plane and contract out-of-plane relative to the arc-melted samples.

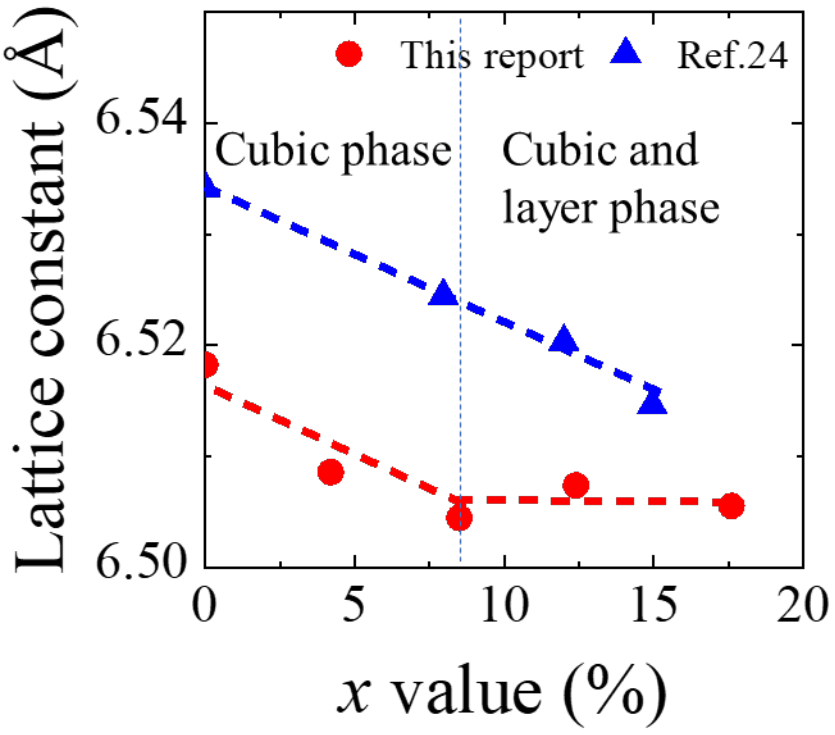

Figure 2. *x* value dependence of the lattice constant for the cubic phase, calculated from the peak position of *210* integrated over the range of ψ = 0–30°. Closed circles and triangles indicate data from this study and from Ref. 24, respectively.

Electrical and thermoelectric properties

Figure 3(a) shows the dependence of the electrical resistivity on the *x* value, measured at room temperature. For comparison, data from the arc-melted samples in Ref. 24 are shown in Figure 3(a). The electrical resistivity continuously decreases with increasing *x* value, deviating from the previous findings, where resistivity remained nearly constant across different *x* values[24]. In the single cubic phase region ($x \leq 0.08$), the electrical resistivity decreases and tends to saturate with

increasing x. The electrical resistivity in the mixed phase region consisting of cubic and layer phases ($0.08 < x < 0.17$) continuously decreases with increasing x, and the film with $x = 0.20$ (layer phase being the major phase), showed almost one order of magnitude lower resistivity than non-doped $SrSi_2$ ($x = 0$). According to our previous report on the layer phase of $Ca_xSr_{1-x}Si_2$, the layer phase is found to be a metallic phase because the resistivity of this film with x=0.19 shows a low value on the order of 100-200 μΩcm for the temperature range of 15-300K and monotonously increased with increasing temperature.[23] Therefore, the electrical resistivity is expected to decrease as the volume fraction of the layer phase increases.

Figure 3(b) presents the temperature dependence of the electrical resistivity for $(Ca_xSr_{1-x})Si_2$ films with x values up to 0.13. The discontinuity of the obtained data were observed at 300K. This is considered to be mainly due to the measurement setups for these two temperature regions, as mentioned in the Method section. This composition region exhibits only a single diffraction peak corresponding to the *210* reflection of the cubic phase, as shown in Fig. 1. Films with $x \leq 0.08$ exhibited lower resistivity than non-doped $SrSi_2$ ($x = 0$) over the entire measured temperature range. Electrical resistivity of $SrSi_2$ film (x=0) rised with increasing the temperature below 100 K. This trend was confirmed in previous paper and is a characteristic feature of the cubic phase. This trend is consistent with the previous cubic phase trend, and the behavior with inflection points appears to be characteristic of the cubic phase. The shift of inflection points to lower temperatures indicates the formation of a solid solution up to $x = 0.08$. In contrast, this hump of the resistivity is not observed for film with x=0.13. This can be explained by the coexistence of a layer phase with low resistivity. This is one evidence that layer phase is coexist with cubic phase for the film with $x = 0.13$.

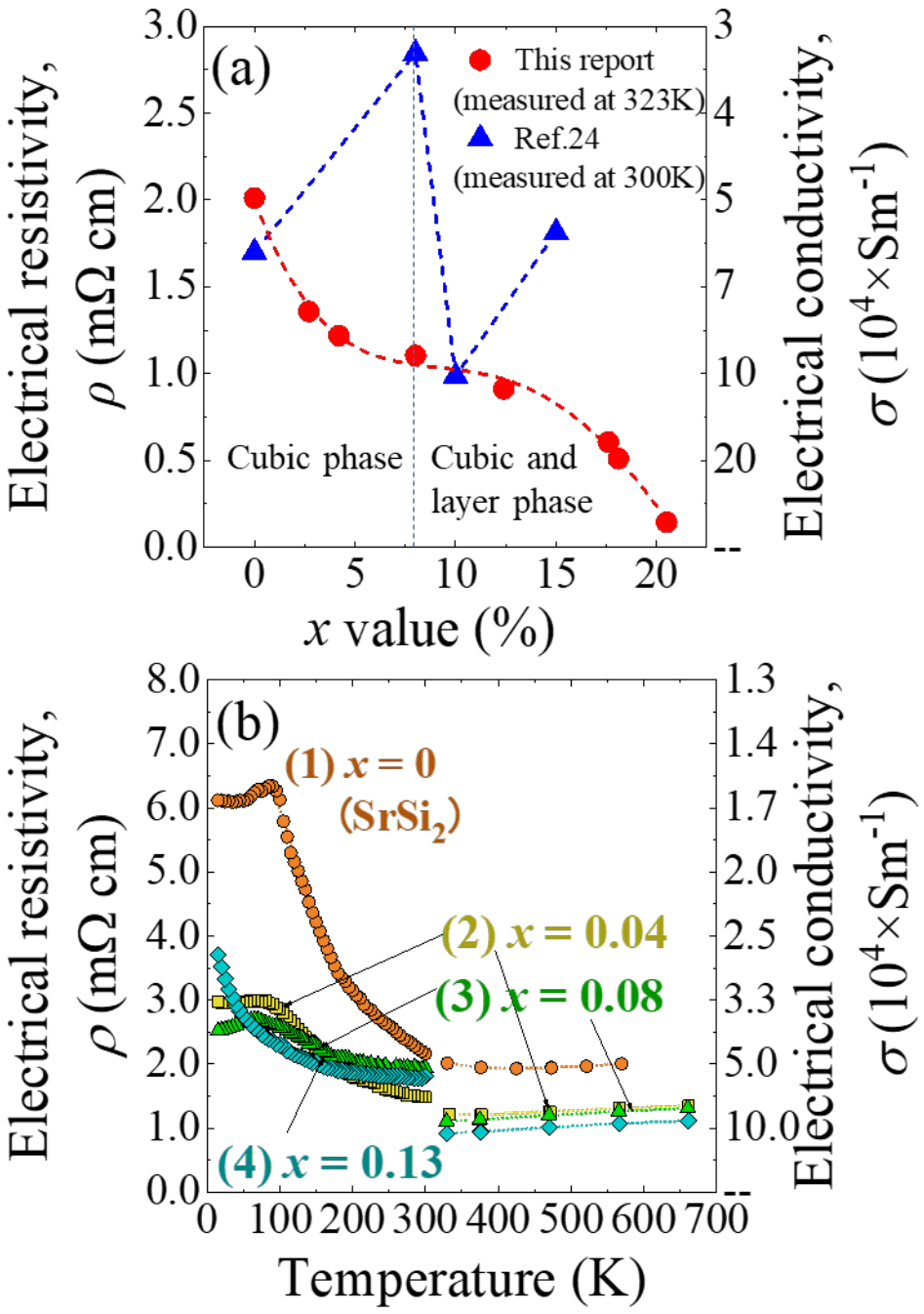

Figure 3. (a) *x* value dependence of electrical resistivity and conductivity measured at room temperature for $(Ca_xSr_{1-x})Si_2$ films (red circles). The closed blue triangles indicate previously reported data from Ref. 24. (b) Temperature dependence of electrical resistivity and conductivity

for the $(Ca_xSr_{1-x})Si_2$ films with (1) $x = 0$ ($SrSi_2$) (closed circles), (2) $x = 0.04$ (closed squares), (3) $x = 0.08$ (closed triangles), and (4) $x = 0.13$ (closed diamonds).

Figure 4 shows the temperature dependence of the logarithm of carrier density below room temperature for the same $(Ca_xSr_{1-x})Si_2$ films presented in Fig. 3(b). An inflection point in carrier concentration is observed around 90 K for $SrSi_2$, and for Ca-substituted films with $x = 0.04$ and 0.08. In contrast, this inflection point is absent in the film with $x = 0.13$. This variation in carrier concentration is reflected in the change in electrical resistivity. Furthermore, the decreasing electrical resistivity at temperatures ranging from 90 to 300 K in Figure 3(b) is mainly due to the increase in carrier density with increasing temperature. Moreover, the carrier concentration increases with increasing x value across the entire temperature range. Notably, the absolute carrier concentration of the film with $x = 0.13$ is more than twice that of the other film compositions across the measured range. According to previous study, the carrier concentration in the layer phase is 100 times higher than that in the cubic phase. Therefore, one possibility is that the carrier concentration may increase in the mixed phase compared to the single cubic phase.

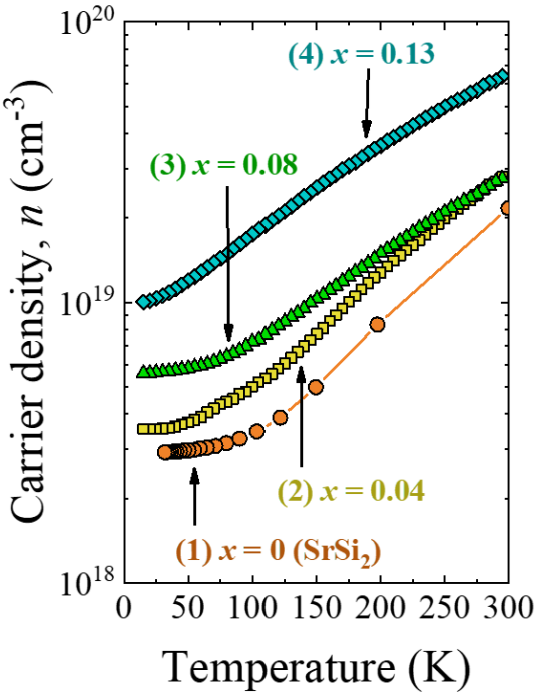

Figure 4. Temperature dependence of carrier density for $(Ca_xSr_{1-x})Si_2$ films with (1) $x = 0$ ($SrSi_2$) (closed circles), (2) $x = 0.04$ (closed squares), (3) $x = 0.08$ (closed triangles), and (4) $x = 0.13$ (closed diamonds).

Figure 5(a) shows the temperature dependence of Hall mobility below room temperature for the same films shown in Figures 3(b) and 4. A continuous decrease in Hall mobility was observed with increasing temperature over the entire temperature range for all films, except for the film with $x = 0.13$. Moreover, the mobility decreases with increasing x for all temperatures. It must be noted that the film with $x = 0.13$ exhibits the lowest mobility among the samples.

Figure 5(b) presents the data shown in Fig. 5(a) on a logarithmic scale of the horizontal axis to investigate the effects of acoustic phonon scattering and impurity scattering on Hall mobility[32]. The slope of all the films above 100 K is approximately -3/2, indicating that mobility depends on

acoustic phonon scattering[32]. Therefore, no noticeable impurity scattering was detected in these films, regardless of the constituent phase. However, impurity scattering appears to dominate below 100 K, as the Hall mobility in the low temperature limit decreases with increasing x.[33,34] The reduced mobility in the film with $x = 0.13$ may be attributed to the presence of mixed phases, which can introduce additional scattering centers.

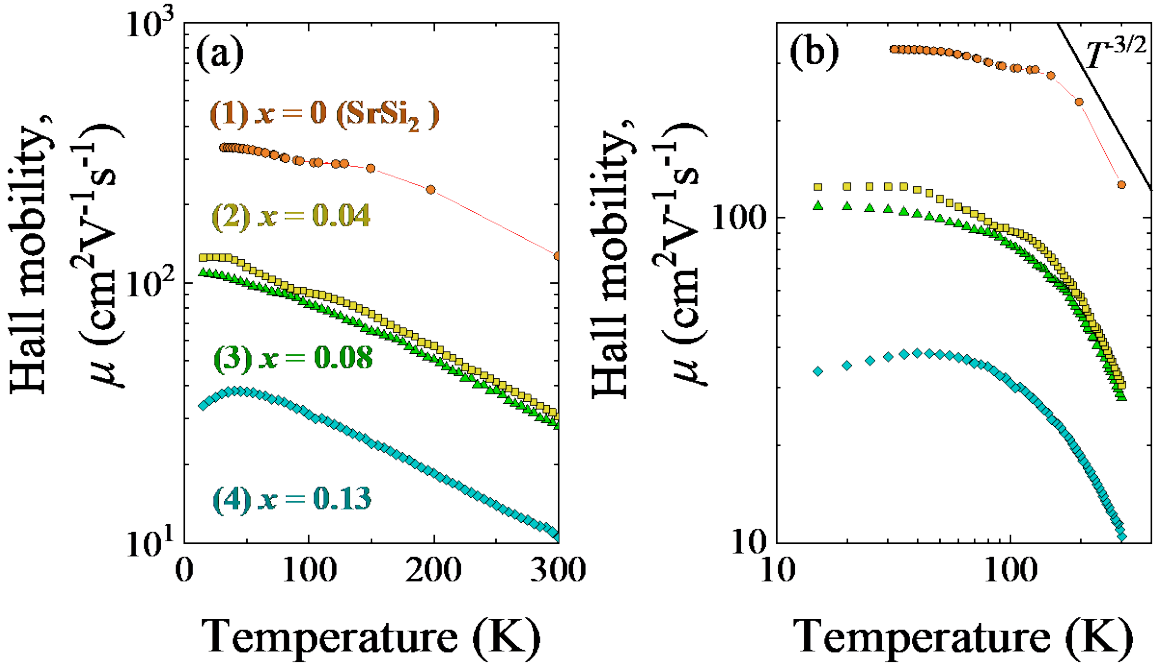

Figure 5. Temperature (T) dependences of Hall mobility (μ) of the $(Ca_xSr_{1-x})Si_2$ films with (1) $x = 0$ ($SrSi_2$) (closed circles), (2) $x = 0.04$ (closed squares), (3) $x = 0.08$ (closed triangles), and (4) $x = 0.13$ (closed diamonds). The vertical and horizontal axes of the graphs were changed for the following considerations: (a) log(μ)-T, (b)log (μ)-Log(T), where T refers to "Temperature".

Figure 6(a) shows the dependence of the Seebeck coefficient on x at 323 K. This temperature was selected to ensure a stable measurement environment with the equipment employed in this study. The positive Seebeck coefficient suggests p-type conduction for films up to $x = 0.17$, where the cubic phase is the majority phase. Within the x range up to 0.08, where a single cubic phase can be obtained, the Seebeck coefficient hardly changes with the x value. This value is almost the same as the reported data for arc-melted $(Ca_xSr_{1-x})Si_2$, except for the anomalous data point at $x = 0.10$ in Fig. 6(a). On the other hand, it decreased with increasing x values for the films consisting of the mixed phase ($x = 0.08$–0.20). Our previously reported $SrSi_2$ films with a cubic phase deposited at 923 K exhibited p-type conduction[24]. Therefore, in this region, the absolute value of the Seebeck coefficient decreased with x in response to the decrease in the volume fraction of the cubic phase. In contrast, the Seebeck coefficient of the film with $x = 0.20$ became negative, which is consistent with the n-type conduction observed in a previous study for the layer phase deposited at 823 K[23].

Figure 6(b) presents the temperature dependence of the Seebeck coefficients of the films shown in Figures 3(b), 4, and 5. A monotonic decrease in the Seebeck coefficient with increasing temperature, along with minimal variation across the compositions, was observed above 323 K across the entire temperature range. In contrast, all $(Ca_xSr_{1-x})Si_2$ films exhibited a maximum Seebeck coefficient below 300 K, with a clear composition dependence on the temperature at which the maximum value was observed. This temperature also coincides with the location of the inflection point of the temperature dependence of Hall mobility. As the temperature increased, the peak became less sharp as the x value increased. The largest Seebeck coefficient value, around 200 μVK^{-1}, was observed for the film with $x = 0.04$. It must be noted that the absolute value of the Seebeck coefficient for the films with $x = 0.13$ is smaller than that of $x =$

0.08. This can be explained by the coexistence of the layered phase, as discussed in Section 1. The simple Seebeck-coefficient mixing model is represented by $|S|_{obsd.} = (\sigma_A|S|_A + \sigma_B|S|_B)/(\sigma_A + \sigma_B)$[35]. Therefore, a mixture of a cubic phase with a high Seebeck coefficient and a layered phase with a low Seebeck coefficient exhibits a lower Seebeck coefficient than a single cubic phase.

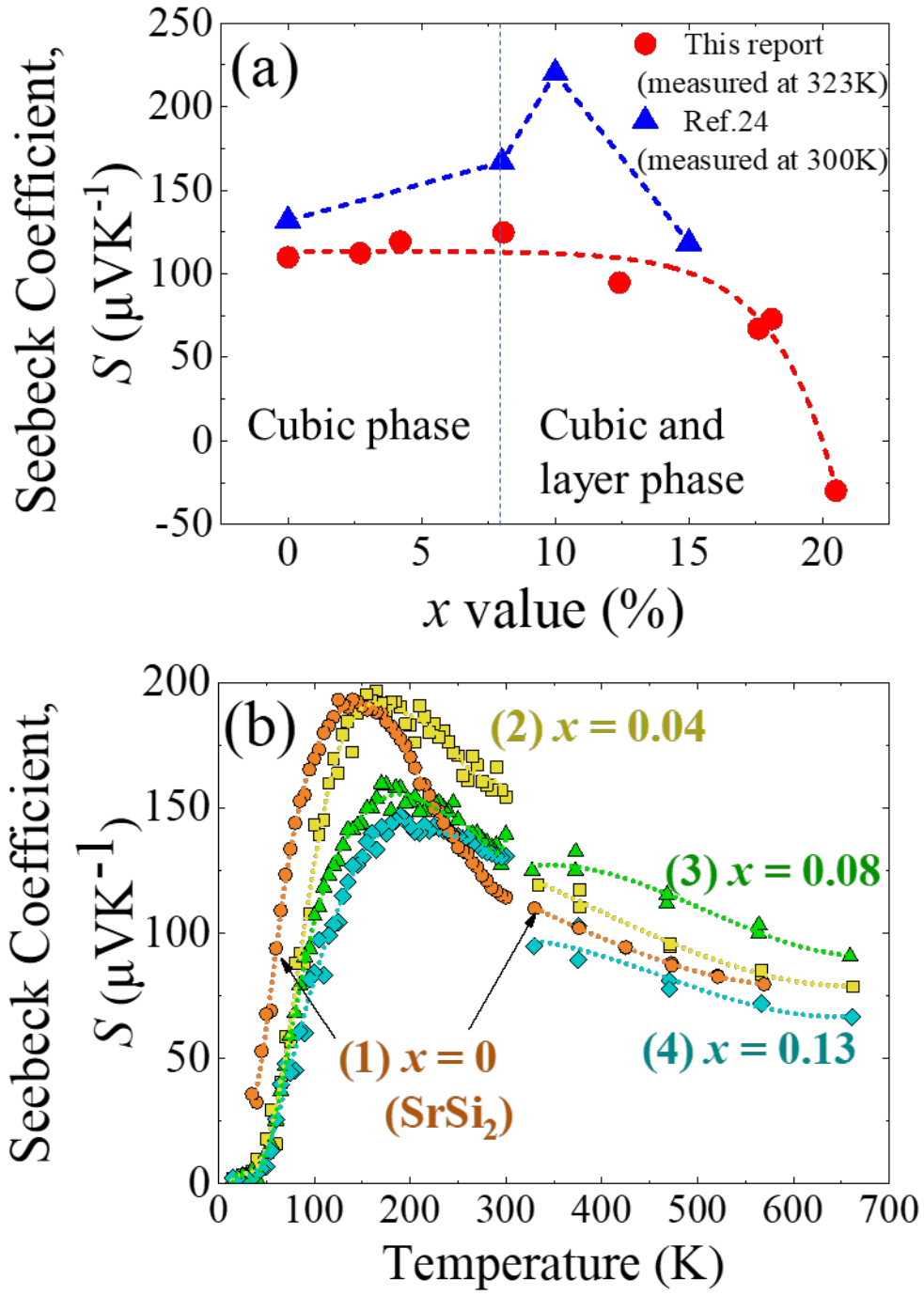

Figure 6. (a) x value dependence of the Seebeck coefficient. The closed red circles and closed blue triangles indicate the present data and the data reported in Ref. 24, respectively. (b) Temperature dependence of the Seebeck coefficient of the $(Ca_xSr_{1-x})Si_2$ films with (1) $x = 0$

($SrSi_2$) (closed circles), (2) x = 0.04 (closed squares), (3) x = 0.08 (closed triangles), and (4) x = 0.13 (closed diamonds).

Figure 7(a) summarizes the x-value dependence of power factors at 323 K. The maximum value near room temperature was observed for the films with x = 0.04. In previous studies, the optimal power factor was established by reducing the resistivity and Seebeck coefficient of the mixed phase. In this case, the solid solution of Ca into the Sr sites reduced the electrical resistivity and Seebeck coefficient of the single cubic phase, resulting in the optimal power factor for the entire thin film in the single-phase region. However, it was confirmed that the effect of the x value on the power factor is not significant. The films with a wide composition range (x = 0.03 to 0.17) exhibited a high value of around 1000 $\mu Wm^{-1}K^{-2}$. This power factor is higher than that of the $(Ba_xSr_{1-x})Si_2$ films reported in our previous study and is comparable to the reported value for the Bi-Te-Se system, which has been extensively investigated in room temperature range[5]. The high power factor maintained over a wide composition range is advantageous for device fabrication, owing to its tolerance to compositional fluctuations. Furthermore, considering that thermal conductivity generally decreases due to solid solution effects and the presence of multiple phases, these films are expected to show an enhanced figure of merit across a wide composition range.

Figure 7(b) shows the temperature dependence of the power factor of $(Ca_xSr_{1-x})Si_2$ films. All $(Ca_xSr_{1-x})Si_2$ films exhibited the maximum value of power factor below 300 K. Especially, the film with x = 0.04 achieved the maximum power factor of approximately 2000 $\mu Wm^{-1}K^{-2}$ at 210 K, which surpasses the maximum values reported in our previous study for pure $SrSi_2$ films

prepared by sputtering method[22,23,25,26]. However, for films with x = 0.08 and 0.13, the temperature dependence of the power factor was nearly identical over the entire temperature range. In the $(Ca_xSr_{1-x})Si_2$ system, an increase in x value increases the electrical conductivity, while the Seebeck coefficient decreases. As a result, the overall power factor does not vary significantly. The power factor for films with x ranging between 0.04 - 0.13 also reached above 850 $\mu Wm^{-1}K^{-2}$ in the temperature range of 223 K- 373 K (near room temperature). Overall, $(Ca_xSr_{1-x})Si_2$ films with a predominantly cubic phase demonstrate significant potential for thermoelectric applications around room temperature, owing to their high and compositionally stable power factor above 850 $\mu Wm^{-1}K^{-2}$ across a wide temperature range.

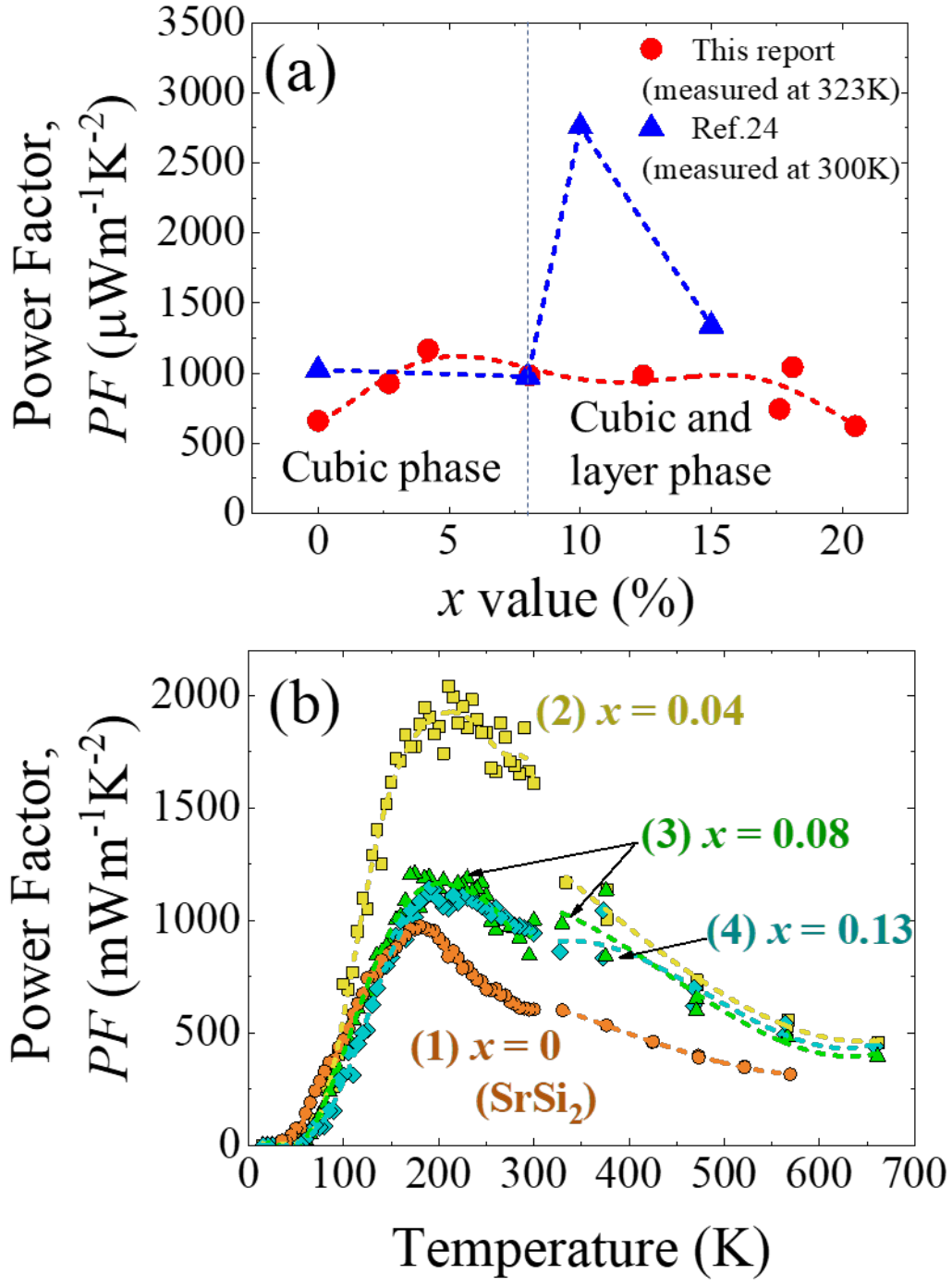

Figure 7. (a) *x* value dependence of the power factor. The closed red circles and blue triangles indicate the present data and those reported in Ref. 24, respectively. (b) Temperature dependence

of the power factor of the $(Ca_xSr_{1-x})Si_2$ films with (1) $x = 0$ ($SrSi_2$) (closed circles), (2) $x = 0.04$ (closed squares), (3) $x = 0.08$ (closed triangles), and (4) $x = 0.13$ (closed diamonds).

Conclusions

We investigated the constituent phases and thermoelectric properties of Ca-substituted $SrSi_2$, $(Ca_xSr_{1-x})Si_2$, films as a function of Ca content. The solubility limit of Ca in the cubic phase was found to be lower in thin films (x = 0.08) compared to arc-melted samples, and a coexistence of cubic and layered phases was observed above x = 0.17, a feature not previously reported in the bulk materials. In both the single-cubic-phase and mixed-phase regions, the electrical resistivity and Seebeck coefficient at 323 K systematically changed with x. As a result, the power factor at 323 K reached around 1000 $\mu Wm^{-1}K^{-2}$ over a wide composition range of x = 0.03 to 0.17. This value was larger than that of our previously reported $(Ba_xSr_{1-x})Si_2$ films, and is comparable to that of the widely studied Bi-Te-Se thermoelectric system near room temperature. Furthermore, a compositionally stable high power factor is advantageous for fabrication, due to its insensitivity to compositional fluctuations. In addition, the power factor for films with x = 0.04-0.13 remained above 850 $\mu Wm^{-1}K^{-2}$ over the temperature range of 223 K-373 K, which covers near room temperature conditions. These findings suggest that $(Ca_xSr_{1-x})Si_2$ films with a predominantly cubic phase are promising candidates for thermoelectric applications near room temperature, owing to their compositionally and temperature stable high power factor above 850 $\mu Wm^{-1}K^{-2}$.

AUTHOR INFORMATION

Corresponding Author

Hiroshi Funakubo

funakubo.h.31df@m.isct.ac.jp

Materials Research Center for Element Strategy, Institute of Science of Technology, Yokohama 226-8502, Japan.

Author Contributions

The manuscript was written through contributions of all authors. All authors have given approval to the final version of the manuscript.

Funding Sources

This work was supported by MEXT Program: Data Creation and Utilization Type, Material Research and Development Project (Grant Number JPMXP1122683430).

All authors have given their approval to the final version of the manuscript.

Notes

The authors declare no competing financial interest.

ABBREVIATIONS

Al_2O_3, aluminum oxide; Ca, calcium; DFT, density functional theory; He, helium; RF, radio frequency; SEM, scanning electron microscopy; Sr, strontium; $SrSi_2$, strontium silicide; XRD, X-ray diffraction; XRF, X-ray fluorescence;

REFERENCES

1 Haras, M.; Skotnicki, T. Thermoelectricity for IoT – A Review. *Nano Energy*. **2018**, 54, 461–476.

2 Zeng, P.; Li, C.; Huang, H.; Gao, Z.; Lan, T.; Chen, K. Research on Thermoelectric Technology for Converter Valves and Test of Energy Harvesting Module. IMCEC, **2024**, 6, 1070–1075.

3 Xiao, F.; Hangarter, C.; Yoo, B.; Rheem, Y.; Lee, K. H.; Myung, N. V. Recent Progress in Electrodeposition of Thermoelectric Thin Films and Nanostructures. *Electrochim. Acta*. **2008**, 53, 8103–8117.

4 Beretta, D.; Neophytou, N.; Hodges, J. M.; Kanatzidis, M. G.; Narducci, D.; Martin- Gonzalez, M.; Beekman, M.; Balke, B.; Cerretti, G.; Tremel, W.; Zevalkink, A.; Hofmann, A. I.; Müller, C.; Dörling, B.; Campoy-Quiles, M.; Caironi, M. Thermoelectrics: from History, a Window to the Future. *Mater. Sci. Eng.: R: Rep.* **2019**, 138, 100501.

5 Cheng, X.; Xu, L.; Liu, W.; Ding, X.; He, W.; Xiao, Y. Progressive Carrier Density Optimization Contributes to Enhanced Thermoelectric Performance in Bi(Te, Se) Compound. *J. Alloys Compd.* **2024**, 972, 172817.

6 Ghannam, R.; Moll, A.; Bérardan, D.; Coulomb, L.; Vieira-E-Silva, A.; Villeroy, B.; Viennois, R.; Beaudhuin, M. Impact of the Nanostructuring on the Thermal and Thermoelectric Properties of α-$SrSi_2$. *J. Alloys Compd.* **2023**, 968, 171876.

7 Ghannam, R.; Coulomb, L.; Moll, A.; Bérardan, D.; Vieira e Silva, A.; Villeroy, B.; Viennois, R.; Beaudhuin, M. *J. Alloys Compd.* **2024**, 147, 107406.

8 Souda, D.; Shimizu, K.; Ohishi, Y.; Muta, H.; Yagi, T.; Kurosaki, K. High Thermoelectric Power Factor of Si–Mg_2Si Nanocomposite Ribbons Synthesized by Melt Spinning. *ACS Appl. Energy Mater.* **2020**, 3, 1962–1968.

9 Faleev, S. V.; Léonard, F. Theory of Enhancement of Thermoelectric Properties of Materials with Nanoinclusions. *Phys. Rev. B*. **2008**, 77, 214304.

10 Szczech, J. R.; Higgins, J. M.; Jin, S. Enhancement of the Thermoelectric Properties in Nanoscale and Nanostructured Materials. *J. Mater. Chem.* **2011**, 21, 4037–4055.

11 Kim, G.; Shin, H.; Lee, J.; Lee, W. A Review on Silicide-Based Materials: Thermoelectric and Mechanical Properties. *Met. Mater. Int.* **2021**, 27, 2205–2219.

12 Liu, H.; Yang, C.; Wang, R. Passive thermal management of electronic devices. *Device*. **2025**, 3, 100684.

13 Chen, H.; Zhang, T.; Gao, Q.; Lv, J.; Chen, H.; Huang, H. Thermal Management Enhancement of Electronic Chips Based on Novel Technologies. *Energy*. **2025**, 316, 134575.

14 Hashimoto, K.; Kurosaki, K.; Imamura, Y.; Muta, H.; Yamanaka, S. Thermoelectric Properties of $BaSi_2$, $SrSi_2$, and LaSi. *J. Appl. Phys.* **2007**, 102, 063703.

15 Kuo, Y. K.; Ramachandran, B.; Lue, C. S. Optimization of Thermoelectric Performance of SrSi2-Based Alloys via the Modification in Band Structure and Phonon-Point-Defect Scattering. *Front. Chem.* **2014**, 2, 106.

16 Imai, M.; Naka, T.; Furubayashi, T.; Abe, H.; Nakama, T.; Yagasaki, K. Electrical properties of polycrystalline $SrSi_2$. *Appl. Phys. Lett.* **2005**, 86, 1–3.

17 Ghannam, R.; Coulomb, L.; Moll, A.; Bérardan, D.; Maurin, D.; Bantignies, J. L.; Mauguin, O.; Vieira e Silva, A.; Rebière, B.; Villeroy, B.; Rouquette, J.; Chevallier, G.; Estournès, C.; Viennois, R.; Beaudhuin, M. A Multiscale Approach to Enhance the Thermoelectric Properties of α-$SrSi_2$ through Micro-/Nano-Structuring and Ba Substitution. *J. Alloys Compd.* **2024**, 1002, 175422.

18 Huang, S. M.; Xu, S. Y.; Belopolski, I.; Lee, C. C.; Chang, G.; Chang, T. R.; Wang, B. K.; Alidoust, N.; Bian, G.; Neupane, M.; Sanchez, D.; Zheng, H.; Jeng, H. T.; Bansil, A.; Neupert, T.; Lin, H.; Hasan, M. Z. New Type of Weyl Semimetal with Quadratic Double Weyl Fermions. *Proc. Natl. Acad. Sci. U. S. A.* **2016**, 113, 1180–1185.

19 Flores-Livas, J. A.; Debord, R.; Botti, S.; San Miguel A.; Pailhès S.; and Marques M. A. L.. Marques. Superconductivity in layered binary silicides: A density functional theory study. *Phys. Rev. B*. **2011**, 84, 1–7.

20 Tokmachev, A. M.; Averyanov, D. V.; Karateev, I. A.; Parfenov, O. E.; Vasiliev, A. L.; Yakunin, S. N.; Storchak, V. G. Topotactic Synthesis of the Overlooked Multilayer Silicene Intercalation Compound $SrSi_2$. *Nanoscale*. **2016**, 8, 16229–16235.

21 Castillo, S. M.; Tang, Z.; Litvinchuk, A. P.; Guloy, A. M. Lattice Dynamics of the Rhombohedral Polymorphs of $CaSi_2$. *Inorg. Chem.* **2016**, 55, 10203–10207.

22 Aoyama, K.; Shimizu, T.; Kuramochi, H.; Mesuda, M.; Akiike, R.; Katase, T.; Kimura, Y.; Funakubo, H. Enhanced Thermoelectric Properties of $SrSi_2$ Composite Films with Cubic and Layered Polymorphs. *ACS Appl. Energy Mater.* **2023**, 6, 6593–6597.

23 Aoyama, K.; Shimizu, T.; Kuramochi, H.; Mesuda, M.; Akiike, R.; Ide, K.; Katase, T.; Kamiya, T.; Kimura, Y.; Funakubo, H. Fabrication and Characterization of $(Ca_xSr_{1-x})Si_2$ Films Prepared by Co-Sputtering Method. *MRS Adv.* **2020**, 5, 451–458.

24 Lue, C. S.; Wong, S. F.; Huang, J. Y.; Hsieh, H. L.; Liao, H. Y.; Ramachandran, B.; Kuo, Y. K. Chemical Pressure Effect on Thermoelectric Properties of Ca and Ba Substituted $SrSi_2$ Alloys. *J. Appl. Phys.* **2013**, 113, 013710.

25 Aoyama, K.; Shimizu, T.; Kuramochi, H.; Mesuda, M.; Akiike, R.; Kimura, Y.; Funakubo, H. Evaluation of Phase and Thermoelectric Properties of Thin Film $SrSi_2$. *J. Ceram. Soc. Japan.* **2019**, 127, 394–398.

26 Aoyama, K.; Shimizu, T.; Kuramochi, H.; Mesuda, M.; Akiike, R.; Ide, K.; Katase, T.; Kamiya, T.; Kimura, Y.; Funakubo, H. Thermoelectric $(Ba_xSr_{1-x})Si_2$ films prepared by sputtering method over the barium solubility limit. *Jpn. J. Appl. Phys.* **2019**, 59, SFFB02.

27 Saito, K.; Oikawa, T.; Kurosawa, T.; Akai, T.; Funakubo, H. Role of Non-180° Domain Switching in Electrical Properties of $Pb(Zr_{0.35},Ti_{0.65})O_3$ Thin Films. *Jpn. J. Appl. Phys.* **2002**, 41, 6730–6734.

28 Katase, T.; Endo, K.; Ohta, H. Room-Temperature-Protonation-Driven On-Demand Metal–Insulator Conversion of a Transition Metal Oxide. *Phys. Rev. B*. **2014**, 90, 1–4.

29 Manfrinetti, P.; Fornasini, M. L.; Palenzona, A. The Phase Diagram of the Ca–Si System. *Intermetallics*. **2000**, 8, 223–228.

30 Nakano, H.; Yamanaka, S.; Hattori, M. Reactivity of RF Magnetron Sputtered $CaSi_2$ Film. *Solid State Ionics*. **1992**, 53–56, 635–640.

31 Brutti, S.; Nguyen-Manh, D.; Pettifor, D. G. Lattice stability of Ca, Sr and Yb disilicides. *Intermetallics*. **2006**, 8, 1472–1486.

32 J. Y. and W. SetoSeto, J. Y. W. The Electrical Properties of Polycrystalline Silicon Films. *J. Appl. Phys.* **1975**, 46, 5247–5254.

33 Katase, T.; Nomoto, S.; He, X.; Kitani, S.; Honda, T.; Hiramatsu, H.; Hosono, H.; Kamiya, T. Simultaneous Realization of Single-Crystal-Like Electron Transport and Strong Phonon Scattering in Polycrystalline $SrTiO_{3-x}H_x$. *ACS Appl. Electron. Mater.* **2024**, 6, 7424–7429.

34 He, X.; Nomoto, S.; Komatsu, T.; Katase, T.; Tadano, T.; Kitani, S.; Yoshida, H.; Yamamoto, T.; Mizoguchi, H.; Ide, K.; Hiramatsu, H.; Kawaji, H.; Hosono, H.; Kamiya, T. Hydride Anion Substitution Boosts Thermoelectric Performance of Polycrystalline $SrTiO_3$ via Simultaneous Realization of Reduced Thermal Conductivity and High Electronic Conductivity. *Adv. Funct. Materials.* **2023**, 33, 2213144.

35 Katase, T.; Endo, K.; Tohei, T.; Ikuhara, Y.; Ohta, H. Room-Temperature-Protonation-Driven On-Demand Metal–Insulator Conversion of a Transition Metal Oxide. *Adv. Elect. Materials.* **2015**, 1, 1500063.

36 Singh, B.; Chang, G.; Chang, TR.; Huang, SM.; Su C.; Lin NC.; Lin H.; Bansil A. Tunable double-Weyl Fermion semimetal state in the $SrSi_2$ materials class. *Sci Rep* **2018**, 8, 10540.

Table of Contents (TOC)